PUBLIC HEALTH
OpenJournal

Openventio
PUBLISHERS

Original Research Article

Beyond Simultaneous Waves: A Critical Review of COVID-19 Epidemic Synchronization and Different Country Transmission Dynamics

Sujith Arokia Swamy B[1,2], Raj Shekar M[1,2], Naveen Kumar P[3], Bhavana Kabber[3], Harish Nayak[4,*]

[1]The Graduate School, ICAR-Indian Agricultural Research Institute, New Delhi, India – 110012
[2]ICAR-Indian Agricultural Statistics Research Institute, New Delhi, India – 110012
[3]University of Agricultural Sciences, Raichur, Karnataka, India – 584104
[4]University of Agricultural Sciences, Dharwad, Karnataka, India – 580005

Corresponding Author
Harish Nayak
Email: harishnayak626@gmail.com

Article Information:
Received: 03 December 2025 | Revised: 05 January 2026 | Accepted: 09 January 2026 | Published: January 16, 2026

Cite this article:
Sujith Arokia Swamy B, Raj Shekar M, Naveen Kumar P, Bhavana Kabber and Harish Nayak (2025). Beyond Simultaneous Waves: A Critical Review of COVID-19 Epidemic Synchronization and Different Country Transmission Dynamics. *Public Health Open Journal*. 10(2):10–23. https://doi.org/10.17140/PHOJ.10.02.10

Abstract
COVID-19 waves peaked at different times in different countries, but the extent to which national epidemics were synchronized, and how synchrony changed as variants, vaccination and policies changed, is rarely quantified with several complementary methods. To compare the timing, duration and magnitude of epidemic waves in ten countries and to evaluate their synchronization using cross-correlation, wavelet coherence, dynamic time warping (DTW), network analysis and time-varying dependence measures, with a random-effects meta-analytic synthesis across countries. A protocol-driven synthesis of a ten-country daily dataset (Australia, Brazil, France, Germany, India, Italy, Japan, South Africa, United Kingdom, United States; 16,751 country-day records, 239 complete weeks, 12 January 2020 to 4 August 2024) was combined with a narrative critical review of the methods. Weekly cases per million were used because the daily series were reported in weekly batches. Four meta-analyses (k = 10) used restricted maximum likelihood with Hartung-Knapp adjustment and prediction intervals. 45 waves were detected. The between-country standard deviation of peak timing (τ) ranged from 3.4 weeks for the Omicron BA.1/BA.2 wave to 9.5 weeks for the Alpha/Beta/Delta period. Mean maximum cross-correlation was 0.72, with 22 of 45 pairs significant after surrogate testing and false-discovery-rate control, and 32 pairs peaking at zero lag. Mean wavelet coherence was 0.43-0.46 across bands, but only 12-18% of the usable time-frequency area was significant. Phase synchrony rose from 0.22 before vaccination to 0.59 in the late period (null mean 0.28). Omicron peaks were 3.6 times earlier peaks (95% CI 1.7-7.6), and the case-fatality ratio was 0.17 times the pre-Omicron ratio (95% CI 0.11-0.27). Synchrony with the other nine countries was high for levels (r = 0.84) and moderate for weekly growth (r = 0.43, I^2 = 78%). Synchrony was partial and episodic rather than constant: strongest for the Omicron wave and late-period dynamics, weakest during the first year and the Alpha/Beta/Delta period. Spatial proximity explained little of the pairwise synchrony. Case-based timing is affected by changes in testing and reporting, so the findings describe reported epidemics rather than true infection incidence.
Keywords: COVID-19; epidemic synchronization; wavelet coherence; dynamic time warping; network epidemiology; random-effects meta-analysis; phase shift

1. Introduction

From 2020 to 2024 every country experienced several COVID-19 waves, yet their timing differed widely: some countries peaked within weeks of one another, whereas others were separated by many months. Understanding why national epidemic waves occur at different times matters for forecasting, for the design of coordinated surveillance, and for judging whether policies in one country can be informed by experience in another. Most quantitative work has asked how many cases will occur, whereas the timing and coordination of waves across countries has received less systematic attention.

Ecological theory provides a vocabulary for this problem. In measles, whooping cough and influenza, epidemics in connected populations show waves that travel with characteristic delays and synchrony that depends on coupling, seasonality and population size (Grenfell et al., 2001; Rohani et al., 1999; Viboud et al., 2006; Bjornstad et al., 1999). For COVID-19, many factors can shift timing: the date and size of introductions, the arrival of variants with different transmissibility (Faria et al., 2021; Tegally et al., 2021; Viana et al., 2022; Volz et al., 2021), non-pharmaceutical interventions (Flaxman et al., 2020; Hale et al., 2021), mobility and travel networks (Chinazzi et al., 2020; Kraemer et al., 2020), seasonal forcing (Baker et al., 2020; Kissler et al., 2020; Neher et al., 2020), vaccination (Mathieu et al., 2021), and changing testing and reporting.

A range of methods can describe synchronization, and each answers a different question. Cross-correlation quantifies linear association at a lag; wavelet coherence resolves association by time and period; dynamic time warping aligns series that are shifted or stretched in time; network epidemiology treats countries as nodes with weighted links; and time-varying dependence measures show whether coupling strengthens or weakens. These methods are rarely applied together to the same data, and their assumptions and failure modes differ. This article therefore has three aims. First, to review critically how these methods have been used to study epidemic synchrony and what can mislead. Second, to apply them to a ten-country COVID-19 dataset and compare the timing, duration and magnitude of waves. Third, to synthesize country-level effects quantitatively through random-effects meta-analysis, with an assessment of heterogeneity.

2. Methods

2.1 Review design and its limits

The study has two components. The first is a protocol-driven quantitative synthesis in which the ten countries are the units of synthesis; it follows the reporting logic of PRISMA 2020 (Page et al., 2021) where applicable (flow of records, eligibility, appraisal of data quality, synthesis, heterogeneity, and sensitivity analysis), as shown in Figure 1. The second is a narrative critical review of the analytical methods. The methodological literature in this article was identified non-systematically, from key texts and from papers on measles, influenza and COVID-19 synchrony; no database search with a registered protocol was run. Section 6 therefore treats the literature component as a critical narrative review, not as a systematic literature search.

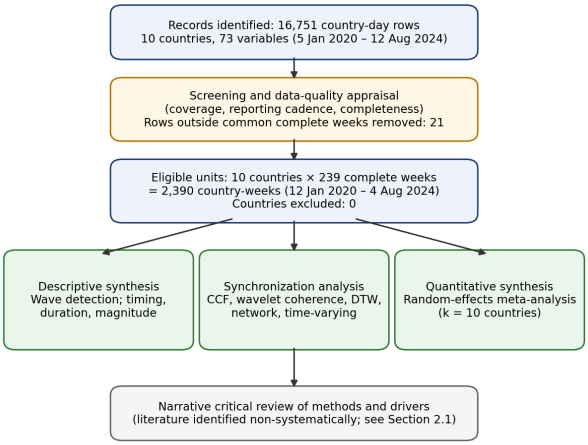


Figure 1. Flow of data through the synthesis (PRISMA-style, adapted to a data synthesis).

2.2 Data source and eligibility

The dataset contains daily country-level records for Australia, Brazil, France, Germany, India, Italy, Japan, South Africa, the United Kingdom and the United States, with 73 variables on cases, deaths, testing, hospitalization, vaccination, policy stringency, demographics and excess mortality. Records run from 5 January 2020 to between 4 and 12 August 2024. The variable structure matches that of the Our World in Data COVID-19 compilation (Mathieu et al., 2020; Mathieu et al., 2021; Hale et al., 2021). All ten countries met the inclusion rule (complete daily coverage with no duplicated dates) and none was excluded.

2.3 Data-quality appraisal and preprocessing

As an analogue of risk-of-bias assessment, each country was appraised for coverage, share of zero-valued days in daily new cases, and availability of testing, hospital, stringency, vaccination, excess-mortality and reproduction-number variables. In every country 86-90% of the days in 2020-2022 had zero reported new

cases, which shows that daily new cases were recorded once per week; daily smoothing and day-level analyses are therefore not valid, and weekly aggregation is lossless. New cases and deaths were summed over calendar weeks ending Sunday, keeping only complete weeks present in all countries (12 January 2020 to 4 August 2024; 239 weeks), converted to incidence per million, and smoothed with a three-week centred mean. For correlation-based and wavelet analyses, log(1 + incidence) was linearly detrended and standardized; weekly growth was the first difference of the smoothed log series.

2.4 Wave detection and wave characteristics

Waves were identified as peaks in smoothed weekly incidence per million using topographic prominence (peak prominence of at least 8% of the country maximum and at least 25 per million; minimum separation six weeks) with the SciPy implementation (Virtanen et al., 2020). Timing was the peak week; duration was the width at half peak height; magnitude was peak incidence per million and cumulative incidence between the prominence bases; growth and decay were log-incidence slopes from base to peak and peak to base. Sensitivity analyses used prominence thresholds of 5% and 15%. For synchronization and meta-analysis, seven a priori windows were defined from dominant epidemiological periods: first wave (March-June 2020), autumn-winter 2020/21, Alpha/Beta/Delta (March-September 2021), Omicron BA.1/BA.2 (28 November 2021-April 2022), summer 2022, winter 2022/23 and 2023/24. The highest smoothed week in each window was the window peak; peaks on a window boundary were treated as indistinct and excluded. Sampling uncertainty of each window peak date was estimated by 300 Poisson parametric bootstrap resamples of the weekly counts, plus the variance of weekly rounding (1/12 week^2).

2.5 Synchronization methods

Cross-correlation. The cross-correlation function of standardized series was computed for lags up to ±26 weeks (Eq. 1), and the maximum absolute value and its lag were retained for each of the 45 pairs.

$r_{xy}(k) = (1/n) \Sigma_t z_x(t) z_y(t + k)$; positive k: x leads y (1)

Because trending and wave-like series produce spurious correlation (Yule, 1926; Granger and Newbold, 1974), significance was assessed against 499 phase-randomized surrogate pairs for each country pair (Theiler et al., 1992; Schreiber and Schmitz, 2000), using the maximum absolute correlation over all lags as the test statistic, with Benjamini-Hochberg false-discovery-rate control (Benjamini and Hochberg, 1995). Correlations of weekly growth were computed as a robustness check.

Wavelet coherence. Squared wavelet coherence was computed with a Morlet wavelet ($\omega_0 = 6$) following Torrence and Compo (1998), Torrence and Webster (1999) and Grinsted et al. (2004), for periods of 4-96 weeks, with time and scale smoothing. Significance (5%) was set per scale from 60 pairs of simulated AR(1) series matching the lag-1 autocorrelation of each series. For three period bands (8-16, 16-32, 32-64 weeks) the mean coherence outside the cone of influence, the proportion of significant area, and the mean phase-derived lead in weeks were computed. Phase was interpreted as a lead only where coherence was significant.

Dynamic time warping. DTW (Berndt and Clifford, 1994) with a Sakoe-Chiba band of 26 weeks (Sakoe and Chiba, 1978) was applied to standardized series; the DTW distance, the mean signed warping offset (positive: the first country's features occur earlier), and average-linkage clustering were obtained. DTW distance was compared with Euclidean distance.

Network epidemiology. An undirected network was formed from country pairs with FDR-significant cross-correlation (edge weight = maximum |r|), and a directed lead-lag network from the sign of the optimal lag. Strength, degree, weighted clustering, and greedy modularity communities (Clauset et al., 2004; Newman, 2006) were computed with NetworkX (Hagberg et al., 2008). Mantel tests with 4,999 permutations (Mantel, 1967) related pairwise synchrony to great-circle distance between capitals, difference in mean policy stringency, difference in median age, difference in log population density, and opposite hemisphere. Geographic proximity is only a proxy for mobility, which is not in the dataset (Balcan et al., 2009; Brockmann and Helbing, 2013; Pastor-Satorras et al., 2015).

Time-varying dependence. Series were band-pass filtered (10-40 weeks; third-order Butterworth, zero-phase), instantaneous phases were obtained with the Hilbert transform (Rosenblum et al., 1996), and the Kuramoto order parameter $R(t) = |N^{-1} \Sigma \exp(i\theta_j(t))|$ measured instantaneous phase synchrony (Kuramoto, 1984; Pikovsky et al., 2001); pairwise phase-locking values were also computed (Lachaux et al., 1999). The first and last 13 weeks were discarded as filter-edge regions. R(t) was compared across four eras (pre–vaccine; vaccine rollout before Omicron; Omicron; late/endemic) with block-bootstrap intervals and a Kruskal-Wallis test, and against 200 phase-randomized surrogate datasets. Mean pairwise correlation in a 52-week sliding window gave a second view.

2.6 Meta-analysis

Effect sizes were computed per country and pooled by random-effects meta-analysis with restricted maximum likelihood estimation of the between-country variance τ^2 (Viechtbauer, 2005), Hartung-Knapp-Sidik-Jonkman confidence intervals with t-distribution (Knapp and Hartung, 2003), and 95% prediction intervals (IntHout et al., 2016). Heterogeneity was summarized by Cochran's Q, τ^2 and I^2 (Higgins and Thompson, 2002; Higgins et al., 2003). Four syntheses were pre-specified: (MA1) log ratio of the Omicron-wave peak to the maximum earlier peak, with variance from Poisson counts in the peak window; (MA2) pooled peak timing and between-country dispersion τ for each window, with the bootstrap variance above; (MA3) Fisher z of each country's correlation with the mean of the other nine countries, for levels (MA3a) and weekly growth (MA3b), with variance 1/(n_eff − 3) and the effective sample size n_eff corrected for autocorrelation (Bayley and Hammersley, 1946); and (MA4) log ratio of the lagged (two-week) case-fatality ratio in the Omicron era (28 November 2021-27 November 2022) to that before Omicron (1 March 2020-21 November 2021). Subgroups were Southern and Northern Hemisphere. Single-covariate meta-regressions (median age, log population density, log GDP per capita, human development index, mean stringency in 2020-2021, hemisphere) were exploratory because k = 10. Leave-one-out analyses, and Egger regression where sampling variances varied, assessed robustness and small-study effects. Analyses used Python with NumPy, SciPy, statsmodels and NetworkX; all tests were two-sided.

Note: sampling variances in MA1 and MA4 derive from Poisson case and death counts and are very small; heterogeneity (I^2) is therefore close to 100% by construction, and τ, together with the prediction interval, is the informative summary of between-country variation. Egger tests and funnel plots are uninformative for these two syntheses.

3. Critical review of methods for epidemic synchronization

Table 1 summarizes what each method measures, its assumptions, and the failure modes most relevant to COVID-19 reported data.

Four lessons from the literature shape the analysis. First, synchrony is scale-dependent: in measles, synchrony and travelling waves differ by period and by spatial scale (Grenfell et al., 2001; Earn et al., 2000; Rohani et al., 1999), which is why methods that resolve period (wavelets) and time (rolling or phase-based measures) are needed in addition to a single correlation. Second, observed synchrony can reflect shared forcing rather than coupling: seasonality, a globally circulating variant, or simultaneous policy relaxation can synchronize otherwise unconnected populations (Bjørnstad et al., 1999; Pikovsky et al., 2001). Third, case reports are not incidence: variation in testing, case definitions and reporting cadence changes both amplitude and apparent timing, an issue that became severe once routine testing declined. Fourth, null models matter. Correlation, coherence and phase-locking all have non-zero expected values for autocorrelated series, so surrogate data are required to say whether synchrony exceeds chance.

4. Results

4.1 Included countries and data quality

Zero-case days of about 86% in every country show that daily new cases were recorded once per week; from 2023 the zero-day share rose to 93-100% in Brazil, Germany, France, Japan and the United States, indicating that reporting moved to a lower frequency or ceased for some days. Availability of testing, hospital and excess-mortality data varied widely, so analyses relied on reported cases and deaths, which were available for all countries. All ten countries were judged adequate for weekly analysis, with the main risk of bias being changes in testing and case ascertainment over time.

4.2 Timing, duration and magnitude of waves

The detection rule found 45 waves across the ten countries (3-6 per country; Figures 2 and 3; Table 4). Counts were sensitive to the prominence threshold: with a 5% threshold 52 waves were detected and with 15% 34. Waves from the Omicron period onward were taller (median peak 7,723 versus 1,969 cases per million per week; Mann-Whitney p = <0.001) and narrower (median half-height width 5.2 versus 7.2 weeks; p = 0.005; Figure 4). Waves rose faster than they decayed (median log-growth 0.160 versus 0.127 per week), although the difference was not significant (Wilcoxon p = 0.160). Width did not differ between hemispheres (medians 6.0 and 5.9 weeks; p = 0.581). Reported deaths followed reported cases with a lag of 0-2 weeks in all countries (maximum cross-correlation 0.69-0.88), which supports the use of case timing as a proxy for epidemic timing within the limits discussed below.

Table 1. Methods for studying epidemic synchronization: assumptions, pitfalls and use in this study.

Method	What it captures	Key assumptions	Principal pitfalls	Key references
Cross-correlation	Linear association and best-fitting lag	Stationarity; linear relation	Spurious correlation for trending or wave-like series; a single lag hides time variation; lag at the search boundary is uninformative	Yule (1926); Granger and Newbold (1974); Theiler et al. (1992)
Wavelet coherence	Association resolved in time and period; phase lead	Adequate length relative to period; red-noise null	Edge effects (cone of influence); short series; smoothing choices; phase interpretable only when coherence is significant	Torrence and Compo (1998); Grinsted et al. (2004); Cazelles et al. (2007, 2008)
Dynamic time warping	Shape similarity allowing shifts and stretching	Elastic alignment is meaningful; window constrains warping	Can match unrelated features if unconstrained; no inference by default; often close to Euclidean distance for similar series	Berndt and Clifford (1994); Sakoe and Chiba (1978)
Network analysis	Structure of pairwise coupling; leaders and communities	Edges are defined by a threshold or test	Edge definition drives structure; correlation is not transmission; confounding by common drivers	Pastor-Satorras et al. (2015); Brockmann and Helbing (2013); Balcan et al. (2009)
Time-varying dependence	Whether coupling changes across eras	Local stationarity within windows	Window length trade-off; phase estimates need narrow-band signals; null models required	Rosenblum et al. (1996); Lachaux et al. (1999); Pikovsky et al. (2001)
Random-effects meta-analysis	Pooled effect and between-country heterogeneity	Exchangeable country effects; known sampling variances	Few units (k = 10); sampling variances ignore ascertainment bias; I^2 misleading when variances are tiny	Borenstein et al. (2009); IntHout et al. (2016)

Table 2. Characteristics of the ten countries.

Country	Population (millions)	Median age	Density (per km^2)	GDP per capita (US$)	HDI	Hemisphere	Cases per million	Deaths per million	Mean stringency 2020-21
Australia	26.2	37.9	3	44,649	0.940	South	453,107	964	63.0
Brazil	215.3	33.5	25	14,103	0.760	South	174,220	3,261	63.6
Germany	83.4	46.6	237	45,229	0.950	North	461,051	2,099	61.1
France	67.8	42.0	123	38,606	0.900	North	575,074	2,479	57.9
United Kingdom	67.5	40.8	273	39,753	0.930	North	369,946	3,438	61.9
India	1417.2	28.2	450	6,427	0.640	North	31,783	377	71.3
Italy	59.0	47.9	206	35,220	0.890	North	453,628	3,342	69.0
Japan	124.0	48.2	348	39,002	0.920	North	272,716	603	43.3
United States	338.3	38.3	36	54,225	0.930	North	305,764	3,527	61.5
South Africa	59.9	27.3	47	12,295	0.710	South	68,000	1,713	58.2

4.3 Why do peaks occur at different times? Window-level timing

Table 5 and Figure 5 give the pooled timing of window peaks. Dispersion of timing varied nearly threefold across windows. The first wave (k = 6) peaked in mid-April 2020 with τ = 3.4 weeks; dispersion rose in autumn-winter 2020/21 (τ = 6.1 weeks, with India first and Brazil last, a range of 18 weeks) and was greatest for Alpha/Beta/Delta (τ = 9.5 weeks; range 24 weeks; Italy first, United States last). The Omicron BA.1/BA.2 wave was the most synchronized (τ = 3.5 weeks, range 13 weeks), with South Africa peaking first (mid-December 2021) and Germany last, consistent with rapid spread from southern Africa (Viana et al., 2022). Dispersion increased again in later windows (τ = 4.2, 6.6 and 6.4 weeks). I^2 was above 99% in every window, as expected when bootstrap sampling variances are small compared with real timing differences; the substantive quantity is τ. Hemisphere effects were inconsistent: Southern Hemisphere countries peaked later than Northern countries in autumn-winter 2020/21 (6.1 weeks) but earlier in summer 2022 (-6.9 weeks), which indicates variant and immunity effects more than a fixed seasonal lag.

Table 3. Data-quality appraisal: share of days with zero reported new cases and availability of selected variables (% of days non-missing).

Country	Zero-case days 2020	2021	2022	2023	2024	Tests	Hospital patients	Stringency	Full vaccination	Excess mortality	Rt
Australia	87	86	86	85	91	100	100	100	100	100	100
Brazil	88	86	86	95	100	100	100	100	100	100	100
Germany	86	86	86	93	100	100	100	100	100	100	100
France	90	86	86	93	100	100	100	100	100	100	100
United Kingdom	87	86	86	85	86	100	100	100	100	100	100
India	88	86	86	85	87	100	100	100	100	100	100
Italy	87	86	86	85	86	100	100	100	100	100	100
Japan	86	86	86	95	100	100	100	100	100	100	100
United States	86	86	86	95	100	100	100	100	100	100	100
South Africa	88	86	86	94	91	100	100	100	100	100	100

Table 4. Wave summary by country.

Country	Waves	Largest peak (per million per week)	Date of largest peak	Median half-height width (weeks)	First detected peak
Australia	4	17,816	2022-01-16	6.2	2022-01-16
Brazil	5	5,471	2022-02-06	6.8	2020-08-09
Germany	5	18,333	2022-03-20	6.4	2020-12-20
France	6	32,975	2022-01-23	4.7	2020-11-01
United Kingdom	4	17,450	2022-01-02	5.4	2021-01-10
India	3	1,817	2021-05-09	6.6	2020-09-20
Italy	5	19,988	2022-01-23	5.9	2020-11-15
Japan	4	11,748	2022-08-14	7.5	2021-08-29
United States	4	15,151	2022-01-16	10.1	2021-01-10
South Africa	5	2,156	2021-12-19	5.8	2020-07-19

4.4 Cross-correlation

Across the 45 country pairs the mean maximum cross-correlation was 0.72 (median 0.74); 25 pairs were significant at the 5% level against phase-randomized surrogates and 22 after false-discovery-rate control (Figure 6; Table 6). The optimal lag was zero for 32 of 45 pairs and at least 10 weeks in absolute value for 5 pairs, all of which involved India or Australia (for example India led Australia by 26 weeks, the search boundary, so that lag should be read as "not estimable within ±26 weeks"). Weekly-growth correlations were lower but followed the same structure (Table 6 footnote). India, Australia and South Africa had the lowest mean correlation with the others (0.57, 0.54 and 0.70), whereas Brazil, France, Germany and the United States had the highest (0.79, 0.79, 0.79 and 0.81). Australia's low values are consistent with near-absent circulation until the Omicron wave.

Mean maximum r for weekly growth was 0.35. Positive lag: the first country leads.

4.5 Wavelet coherence

Mean wavelet coherence was 0.43, 0.46 and 0.40 in the 8-16, 16-32 and 32-64-week bands, but the significant fraction of usable time–frequency area was only 18%, 17% and 12% (Figures 7 and 8; Table 7). Synchrony was therefore patchy: pairs such as Brazil-United States showed extended significant coherence at 8-32 weeks, whereas France-South Africa showed little. Where phase could be interpreted, leads were small (for example the United States led Brazil by about 1.3 weeks in the 16-32-week band), and rank agreement between wavelet-based and cross-correlation leadership was weak (Spearman $\rho = 0.39$).

4.6 Dynamic time warping

DTW distances were strongly correlated with Euclidean distances (Spearman $\rho = 0.93$), so elastic alignment changed the ordering of pairs little in this set of series with similar wave counts. Average-linkage clustering (three clusters) separated {India, South Africa}, {Brazil, Germany, France, United Kingdom, Italy, Japan, United States} and {Australia} (Figure 9). The closest pairs were

Table 5. Random-effects pooled peak timing and dispersion for each a priori window.

Window	k	Pooled peak date	τ (weeks)	I^2 (%)	Range (weeks)	First	Last	Southern minus Northern (weeks)
W1 First wave	6	2020-04-16	3.4	99	9	AUS	FRA	–
W2 Autumn–winter 2020/21	9	2020-12-09	6.1	100	18	IND	BRA	6.1
W3 Alpha/Beta/ Delta	9	2021-05-27	9.5	100	24	ITA	USA	-2.6
W4 Omicron BA.1/BA.2	10	2022-01-25	3.5	99	13	ZAF	DEU	-2.3
W5 Summer 2022 (BA.4/5)	10	2022-07-06	4.2	100	13	AUS	JPN	-6.9
W6 Winter 2022/23	9	2023-01-09	6.6	100	19	FRA	IND	1.0
W7 2023/24	4	2023-11-19	6.4	100	13	GBR	IND	–

Table 6. Ten strongest pairwise cross-correlations (levels).

Pair	Max r	Lag (weeks)	Zero-lag r	p (surrogate)	p (FDR)
BRA–USA	0.94	0	0.94	0.002	0.006
DEU–FRA	0.92	0	0.92	0.002	0.006
DEU–USA	0.91	0	0.91	0.002	0.006
DEU–JPN	0.89	0	0.89	0.002	0.006
BRA–FRA	0.89	0	0.89	0.002	0.006
FRA–USA	0.89	0	0.89	0.002	0.006
JPN–USA	0.87	0	0.87	0.002	0.006
BRA–JPN	0.86	0	0.86	0.002	0.006
FRA–JPN	0.85	0	0.85	0.008	0.020
DEU–ITA	0.85	0	0.85	0.002	0.006

BRA-USA (1.9), DEU-FRA (2.2), DEU-JPN (3.0); the most distant involved Australia (AUS-BRA (11.9), AUS-ZAF (12.5), AUS-IND (13.4)). Leadership rankings from DTW agreed with those from cross-correlation (ρ = 0.91) but not with wavelet phase (ρ = 0.35). DTW distance was related to geographic distance (Mantel ρ = -0.42, p = 0.043; not adjusted for multiple tests).

4.7 Network epidemiology

The FDR-significant synchrony network had 22 edges (density 0.49) and three communities (modularity 0.11): {Germany, France, Italy, Japan, United States}, {Brazil, United Kingdom, India, South Africa}, {Australia} (Figure 10; Table 8). Australia was isolated. Edge structure did not follow geography: synchrony was not significantly associated with great-circle distance (Mantel ρ = -0.28, p = 0.220), hemisphere (ρ = -0.12, p = 0.538), difference in policy stringency (ρ = -0.09, p = 0.750), difference in log population density (ρ = -0.33, p = 0.126) or difference in median age (ρ = -0.30, p = 0.066). Directed lead–lag links were few, because most pairs had zero optimal lag, and net leadership scores were near zero for all countries except France (-0.77) and South Africa (0.77); leadership is therefore not a stable feature of this network.

4.8 Time-varying dependence

Phase synchrony changed markedly over time (Figure 11; Table 9). Mean R(t) was 0.22 before vaccination, 0.52 during vaccine rollout before Omicron, 0.46 in the Omicron era and 0.59 in the late period (Kruskal-Wallis p < 0.001). The overall mean (0.47) was above the mean of phase-randomized surrogates (0.28; 95th percentile 0.35), and the late-period interval lay above the surrogate 95th percentile, so synchrony exceeded chance especially after 2021. The mean phase-locking value across pairs was 0.31. Before vaccination, mean R(t) was below the surrogate mean; the intervals for the vaccine-rollout and late eras lay above the surrogate 95th percentile, and the lower limit for the Omicron era (0.33) was just below it. Sliding-window correlations of levels fluctuated more widely (about 0 to 0.7) than correlations of weekly growth (about 0.1-0.3), which shows that the apparent strength of dependence depends on whether levels or changes are used.

4.9 Meta-analysis

Table 11 and Figure 12 give the pooled results. Magnitude (MA1). Omicron-wave peaks were 3.6 times the largest earlier peak (95% CI 1.7 to 7.6; p = 0.003), but

Table 7. Five strongest pairs in each period band: mean coherence, significant area and phase lead (weeks; positive: first country leads).

Band (weeks)	Pair	Mean coherence	Significant area	Phase lead (weeks)
8-16	JPN-USA	0.78	70%	-0.2
8-16	DEU-FRA	0.66	42%	-0.5
8-16	BRA-USA	0.62	46%	-0.0
8-16	FRA-ITA	0.56	38%	0.3
8-16	GBR-ITA	0.55	27%	0.4
16-32	BRA-USA	0.78	72%	-1.3
16-32	IND-USA	0.73	65%	-1.6
16-32	FRA-ITA	0.66	44%	0.2
16-32	JPN-USA	0.66	48%	-1.5
16-32	BRA-JPN	0.64	43%	1.1
32-64	BRA-ZAF	0.73	51%	-1.0
32-64	FRA-USA	0.73	40%	-5.0
32-64	DEU-GBR	0.67	46%	-5.3
32-64	DEU-USA	0.64	42%	-4.1
32-64	DEU-FRA	0.63	43%	1.3

Table 8. Network metrics by country.

Country	Degree	Strength	Weighted clustering	Community	Lead–lag score (cross-correlation)	Mean DTW distance
Australia	0	0.00	0.00	3	-4	10.8
Brazil	7	5.87	0.47	2	-1	5.5
Germany	5	4.42	0.75	1	-1	5.0
France	6	5.09	0.61	1	-2	5.4
United Kingdom	4	3.22	0.58	2	3	5.9
India	2	1.43	0.80	2	4	8.4
Italy	4	3.23	0.59	1	2	6.7
Japan	4	3.47	0.93	1	-4	6.6
United States	7	6.02	0.56	1	0	5.6
South Africa	5	3.90	0.52	2	3	6.4

between-country variation was large (τ = 1.03; prediction interval 0.30 to 44.2): the ratio was below one in India, where the 2021 wave was larger, and 30-fold in Australia. Synchrony (MA3). Country levels correlated with the mean of the other nine countries at r = 0.84 (95% CI 0.74 to 0.91; I^2 = 0%), but weekly growth rates correlated at only r = 0.43 (95% CI 0.29 to 0.56; I^2 = 78%; prediction interval -0.03 to 0.74), with South Africa lowest (r = 0.07) and the United States highest (r = 0.70). Severity (MA4). The lagged case-fatality ratio in the Omicron era was 0.17 times the pre-Omicron ratio (95% CI 0.11 to 0.27; prediction interval 0.03 to 0.85), consistent with lower severity per reported case in the Omicron period (Nyberg et al., 2022) but also with greater case ascertainment of mild infections and vaccination. Timing (MA2) is given in Table 5. Hemisphere subgroups did not differ for any synthesis (Q-between p = 0.849, 0.623, 0.262 and 0.406). Leave-one-out pooled estimates stayed within 2.9-4.3 (MA1), 0.39-0.47 (MA3b) and 0.15-0.19 (MA4), and Egger tests for MA3 were not significant (p = 0.318 and 0.371).

Eighteen meta-regressions were run with k = 10 countries; none of the associations should be treated as confirmatory, and the p-values are not adjusted for multiplicity. Associations with the human development index and GDP in MA1, and with median age in MA4, were nominally significant and plausibly reflect differences in testing capacity and in the age structure of pre-Omicron mortality; they cannot separate these explanations.

4.10 Sensitivity analyses

Results were stable to the wave-detection threshold for qualitative conclusions (waves per country changed by 0-5 across thresholds; Section 4.2). Excluding any single country did not change the direction or significance of MA1, MA3 or MA4. Growth-based synchrony was lower than level-based synchrony because trending levels share common wave structure that is removed by differencing; conclusions about "high synchrony" therefore depend on the measure used. DTW and Euclidean orderings agreed closely (ρ = 0.93).

Table 9. Phase synchrony R(t) by era (block-bootstrap 95% interval) and mean sliding-window correlation of levels.

Era	Weeks	Mean R(t)	95% interval	Mean sliding-window r
Pre-vaccine	38	0.22	0.14-0.25	0.45
Vaccine rollout, pre-Omicron	47	0.52	0.37-0.66	0.21
Omicron	57	0.46	0.33-0.60	0.32
Late/endemic	71	0.59	0.55-0.69	0.47

Table 10. Mantel tests of pairwise cross-correlation (maximum r) against pairwise covariate differences.

Covariate (pairwise)	Spearman ρ	p (4,999 permutations)
Great-circle distance	-0.28	0.220
Difference in stringency	-0.09	0.750
Difference in median age	-0.30	0.066
Opposite hemisphere	-0.12	0.538
Difference in log density	-0.33	0.126

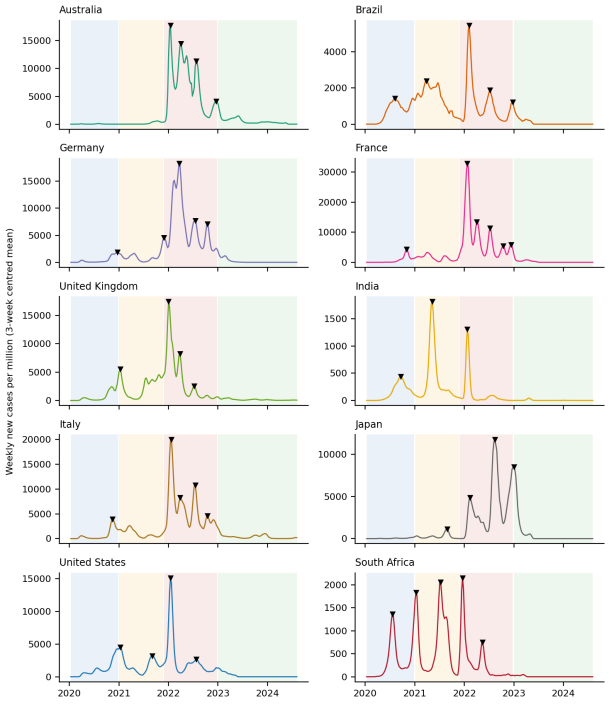


Figure 2. Weekly new cases per million (three-week centred mean) in the ten countries; triangles mark detected wave peaks; background colours mark eras (blue, pre-vaccine; yellow, vaccine rollout before Omicron; red, Omicron; green, late/endemic).

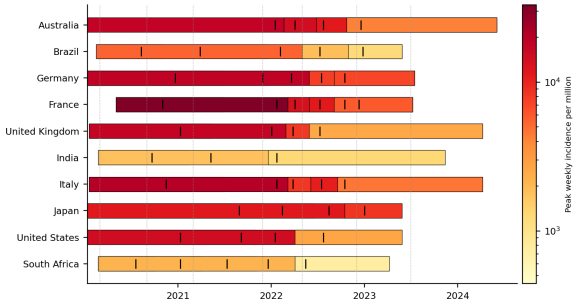


Figure 3. Timeline of detected waves (bars span prominence bases; vertical tick = peak; colour = peak incidence per million). Dotted lines mark the start of the a priori windows.

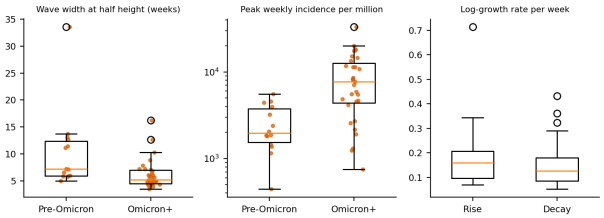


Figure 4. Wave width, peak height and growth/decay rate, pre-Omicron versus Omicron-period and later waves.

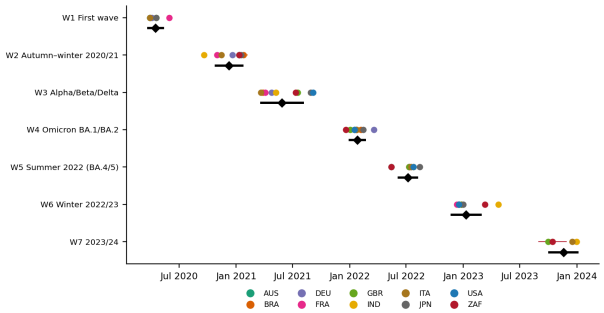


Figure 5. Window peak dates by country (points with bootstrap ± 1 SE) and pooled mean ± τ (black diamond and bar).

5. Discussion

Waves occurred at different times because national epidemics were driven by processes that were only partly shared. The timing analysis shows that synchrony was episodic. Before widespread vaccination, and during the Alpha/Beta/Delta period, peaks were separated by up to 18-24 weeks and between-country dispersion was highest; this is the period when variants arose and spread from different seeding points (Faria et al., 2021; Tegally et al., 2021; Volz et al., 2021), when national policies diverged most (Flaxman et al., 2020; Hale et al., 2021), and when travel was restricted (Chinazzi et al., 2020; Kraemer et al., 2020). The Omicron BA.1/BA.2 wave was the most synchronized. Its high transmissibil-

Table 11. Random-effects meta-analyses across countries (k = 10; REML with Hartung–Knapp adjustment).

Synthesis (effect)	Pooled	95% CI	95% prediction interval	τ^2	I^2 (%)	Q p	Hemisphere Q-between p
MA1: Omicron peak / earlier peak (ratio)	3.63	1.73 to 7.60	0.30 to 44.20	1.069	100	<0.001	0.849
MA3a: synchrony, levels (r)	0.84	0.74 to 0.91	0.73 to 0.91	0.000	0	0.493	0.623
MA3b: synchrony, growth (r)	0.43	0.29 to 0.56	-0.03 to 0.74	0.041	78	<0.001	0.262
MA4: CFR Omicron / pre-Omicron (ratio)	0.17	0.11 to 0.27	0.03 to 0.85	0.441	100	<0.001	0.406

Table 12. Exploratory single-covariate meta-regressions (covariates standardized; log scale for density and GDP; k = 10).

Synthesis	Covariate	Coefficient	95% CI	p
MA1 (peak ratio)	Median age	0.56	-0.10 to 1.22	0.086
MA1 (peak ratio)	Log population density	-0.51	-1.19 to 0.17	0.125
MA1 (peak ratio)	Log GDP per capita	0.75	0.23 to 1.27	0.010
MA1 (peak ratio)	Human development index	0.77	0.27 to 1.27	0.007
MA1 (peak ratio)	Mean stringency 2020–21	-0.18	-0.96 to 0.61	0.617
MA1 (peak ratio)	Southern Hemisphere	0.20	-1.54 to 1.94	0.797
MA3b (growth synchrony)	Median age	0.10	-0.06 to 0.26	0.195
MA3b (growth synchrony)	Log population density	0.02	-0.15 to 0.20	0.757
MA3b (growth synchrony)	Log GDP per capita	0.10	-0.06 to 0.26	0.199
MA3b (growth synchrony)	Human development index	0.10	-0.07 to 0.26	0.212
MA3b (growth synchrony)	Mean stringency 2020–21	-0.02	-0.20 to 0.16	0.826
MA3b (growth synchrony)	Southern Hemisphere	-0.20	-0.55 to 0.16	0.234
MA4 (CFR ratio)	Median age	-0.52	-0.81 to -0.23	0.003
MA4 (CFR ratio)	Log population density	-0.05	-0.56 to 0.46	0.819
MA4 (CFR ratio)	Log GDP per capita	-0.41	-0.80 to -0.02	0.040
MA4 (CFR ratio)	Human development index	-0.45	-0.81 to -0.08	0.022
MA4 (CFR ratio)	Mean stringency 2020–21	0.14	-0.36 to 0.64	0.545
MA4 (CFR ratio)	Southern Hemisphere	0.35	-0.74 to 1.43	0.483

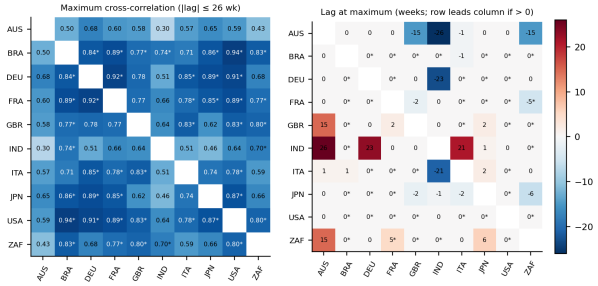


Figure 6. Maximum cross-correlation and lag (weeks) for all pairs; * FDR-adjusted p < 0.05 against phase-randomized surrogates.

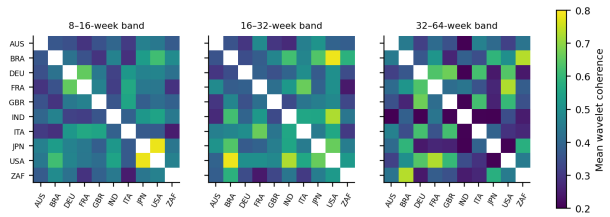


Figure 7. Mean squared wavelet coherence for each country pair, by period band.

ity and immune escape, together with connected populations that had largely relaxed controls, can reduce differences in timing, and the rapid global spread from southern Africa is documented genomically (Viana et al., 2022). The phase-based measure shows that synchrony stayed above the surrogate level after 2021, which is consistent with a shared driver (a common variant, seasonal forcing and immunity) as well as with coupling; these cannot be separated without mobility or genomic data (Pikovsky et al., 2001; Bjørnstad et al., 1999).

The results do not support a simple geographic explanation. Proximity, hemisphere, policy-stringency similarity, density and age similarity

ISSN: 2472-3878 | Vol 10 | Issue 2 | 2025

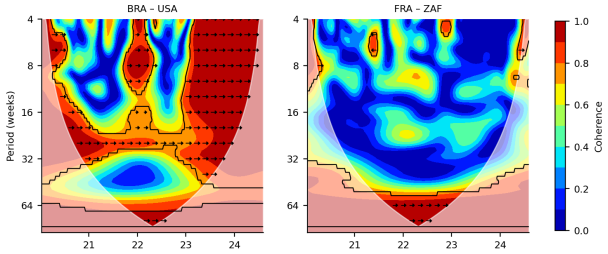


Figure 8. Wavelet coherence for the pair with the highest (Brazil–United States) and lowest (France–South Africa) coherence in the 16-32- week band; black contours: 5% significance; shaded: cone of influence; arrows: phase (right = in phase).

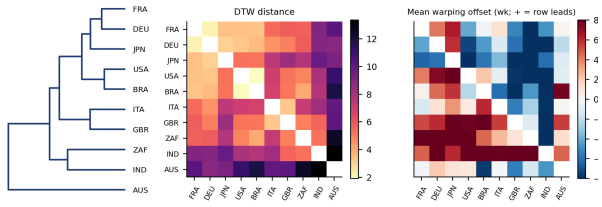


Figure 9. DTW dendrogram, distance matrix and mean warping offset between countries (weeks).

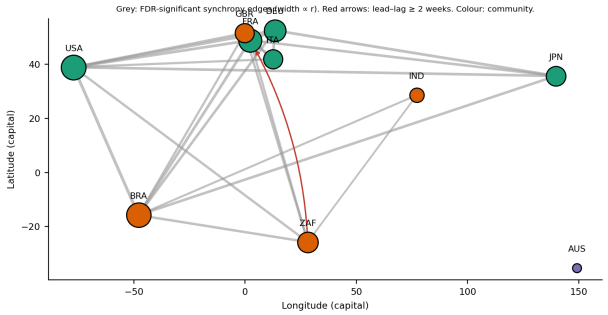


Figure 10. Synchrony network of the ten countries (capital coordinates).

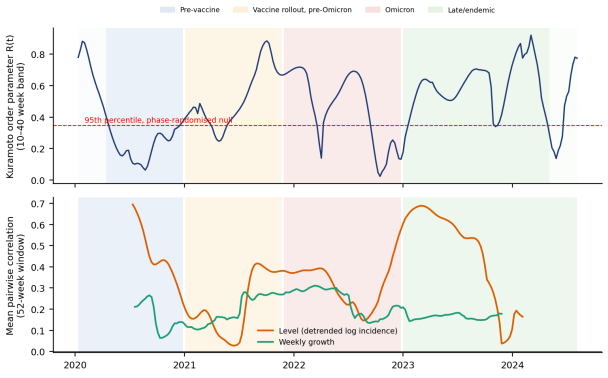


Figure 11. Top: Kuramoto order parameter R(t) (10–40-week band; shaded white areas are filter-edge regions excluded from summaries). Bottom: mean pairwise correlation in a 52-week window.

were not significantly related to pairwise synchrony. The DTW–distance association ($\rho \approx -0.42, p = 0.043$) *was weak evidence and unadjusted for multiple tests. This is consistent with distance–connectivity, not only adjacency, determines the*

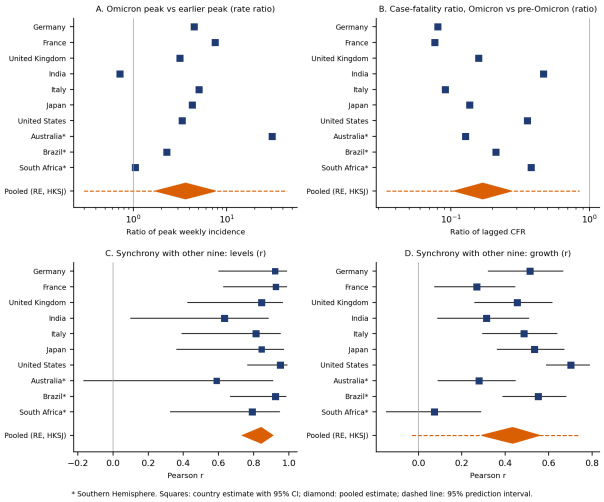


Figure 12. Forest plots for MA1, MA4, MA3a and MA3b (country estimates, pooled estimate and prediction interval; * Southern Hemisphere).

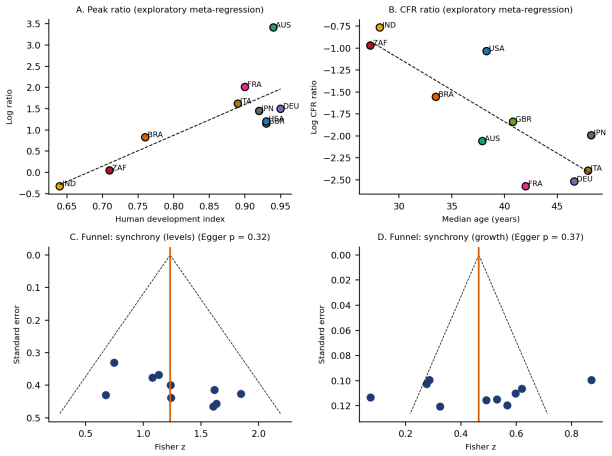


Figure 13. Exploratory meta-regressions and funnel plots (MA3).

Comparing methods is itself an outcome. Cross-correlation gave a clear overall picture (high correlations, mostly zero lag) but cannot show how synchrony changes; wavelet coherence showed that significant coherence occupied only a minority of the time–frequency plane; and the phase-based measure showed when synchrony rose. DTW added little beyond Euclidean distance for series of similar structure, and its warping offsets agreed with cross-correlation leadership but not with wavelet phase. Leadership rankings therefore depend on method, and the data do not support stable "leader" countries other than a tendency for South Africa to lead in the Omicron wave. Practitioners should use more than one method and test against surrogate nulls (Theiler et al., 1992).

The meta-analytic results show that most quantities of interest vary substantially between countries. Peak sizes during Omicron relative to earlier peaks, and the change in case-fatality ratio, had wide prediction intervals, which means that a pooled estimate *This is consistent with* (Borenstein et al., 2013; Balcane

should not be applied to a new country. In MA1 and MA4 the near-100% I^2 follows from very small Poisson sampling variances; the prediction intervals and τ are the informative summaries. Synchrony of weekly growth (MA3b) had moderate heterogeneity ($I^2 \approx 78\%$), whereas synchrony of levels was homogeneous, which is expected because shared multi-wave structure dominates levels.

6. Limitations

Reported cases are not incidence. Changes in testing policy, case definitions and reporting frequency, and the decline in routine testing from 2022, alter amplitude and may shift apparent timing. The Omicron-era peak ratio (MA1) and the case-fatality ratio (MA4) are particularly sensitive to this. Deaths followed cases at 0-2 weeks, but excess-mortality data were incomplete.

Few units. Meta-analysis with k = 10 has low power for heterogeneity tests, subgroup comparisons and meta-regression; Egger tests are unreliable at this size; and the meta-regressions are exploratory and unadjusted for multiple testing.

Variance models. Sampling variances used Poisson counts and bootstrap rounding. They exclude ascertainment error, so confidence intervals are too narrow, and heterogeneity is overstated relative to a model that included such error.

Not a database-searched systematic review. The literature component is a narrative critical review. The quantitative synthesis is systematic with respect to the data (all countries, pre-specified outcomes and windows), but it does not replace a protocol-registered review of published studies.

Method limits. Wavelet coherence is unreliable near series ends and for periods approaching the series length; DTW used one band width; the network used a threshold on FDR-adjusted surrogate tests; hemisphere and distance are crude proxies for mobility and climate; and no genomic, mobility or climate data were included.

Time-varying measures. Phase synchrony requires a narrow band and discards edge weeks, and the era boundaries were chosen from dominant variant periods, not estimated.

Unverified provenance. The dataset was analyzed as supplied; its provenance and any preprocessing should be documented in the final manuscript.

7. Conclusions

Synchronization of COVID-19 waves across ten countries was partial, episodic and method-dependent. Timing dispersion was smallest for the Omicron BA.1/BA.2 wave (τ= 3.5 weeks) and largest for the Alpha/Beta/Delta period (τ = 9.5 weeks); phase synchrony increased after 2020 and exceeded the surrogate null in later eras; and pairwise synchrony was not explained by distance, hemisphere, stringency, age or density. Omicron-era waves were taller and narrower than earlier waves, and the case-fatality ratio fell to about 0.17 of its pre-Omicron value. For forecasting and coordination, the findings imply that cross-country lead times are unstable, so a country's peak is a weak predictor of another's outside periods dominated by a common variant, and that multi-method analyses with surrogate nulls are needed before claiming synchrony or leadership.

References

Baker, R. E., Yang, W., Vecchi, G. A., Metcalf, C. J. E., and Grenfell, B. T. (2020). Susceptible supply limits the role of climate in the early SARS-CoV-2 pandemic. Science, 369(6501), 315-319.

Balcan, D., Colizza, V., Gonçalves, B., Hu, H., Ramasco, J. J., and Vespignani, A. (2009). Multiscale mobility networks and the spatial spreading of infectious diseases. Proceedings of the National Academy of Sciences, 106(51), 21484-21489.

Bayley, G. V., and Hammersley, J. M. (1946). The "effective" number of independent observations in an autocorrelated time series. Supplement to the Journal of the Royal Statistical Society, 8(2), 184-197.

Benjamini, Y., and Hochberg, Y. (1995). Controlling the false discovery rate: A practical and powerful approach to multiple testing. Journal of the Royal Statistical Society: Series B, 57(1), 289-300.

Berndt, D. J., and Clifford, J. (1994). Using dynamic time warping to find patterns in time series. In Proceedings of the AAAI Workshop on Knowledge Discovery in Databases, 359-370.

Bjørnstad, O. N., Ims, R. A., and Lambin, X. (1999). Spatial population dynamics: Analyzing patterns and processes of population synchrony. Trends in Ecology and Evolution, 14(11), 427-432.

Borenstein, M., Hedges, L. V., Higgins, J. P. T., and Rothstein, H. R. (2009). Introduction to meta-analysis. Wiley.

Brockmann, D., and Helbing, D. (2013). The hidden geometry of complex, network-driven contagion phenomena. Science, 342(6164), 1337-1342.

Cazelles, B., Chavez, M., Berteaux, D., Ménard, F., Vik, J. O., Jenouvrier, S., and Stenseth, N. C. (2008). Wavelet analysis of ecological time series. Oecologia, 156(2), 287-304.

Cazelles, B., Chavez, M., de Magny, G. C., Guégan, J.-F., and Hales, S. (2007). Time-dependent spectral analysis of epidemiological time-series with wavelets. Journal of the Royal Society Interface, 4(15), 625-636.

Chinazzi, M., Davis, J. T., Ajelli, M., Gioannini, C., Litvinova, M., Merler, S., Pastore y Piontti, A., Mu, K., Rossi, L., Sun, K., Viboud, C., Xiong, X., Yu, H., Halloran, M. E., Longini, I. M., and Vespignani, A. (2020). The effect of travel restrictions on the spread of the 2019 novel coronavirus (COVID-19) outbreak. Science, 368(6489), 395-400.

Clauset, A., Newman, M. E. J., and Moore, C. (2004). Finding community structure in very large networks. Physical Review E, 70(6), 066111.

Earn, D. J. D., Rohani, P., Bolker, B. M., and Grenfell, B. T. (2000). A simple model for complex dynamical transitions in epidemics. Science, 287(5453), 667-670.

Faria, N. R., Mellan, T. A., Whittaker, C., Claro, I. M., Candido, D. d. S., Mishra, S., et al. (2021). Genomics and epidemiology of the P.1 SARS-CoV-2 lineage in Manaus, Brazil. Science, 372(6544), 815-821.

Flaxman, S., Mishra, S., Gandy, A., Unwin, H. J. T., Mellan, T. A., Coupland, H., et al. (2020). Estimating the effects of non-pharmaceutical interventions on COVID-19 in Europe. Nature, 584(7820), 257-261.

Granger, C. W. J., and Newbold, P. (1974). Spurious regressions in econometrics. Journal of Econometrics, 2(2), 111-120.

Grenfell, B. T., Bjørnstad, O. N., and Kappey, J. (2001). Travelling waves and spatial hierarchies in measles epidemics. Nature, 414(6865), 716-723.

Grinsted, A., Moore, J. C., and Jevrejeva, S. (2004). Application of the cross wavelet transform and wavelet coherence to geophysical time series. Nonlinear Processes in Geophysics, 11(5/6), 561-566.

Hagberg, A. A., Schult, D. A., and Swart, P. J. (2008). Exploring network structure, dynamics, and function using NetworkX. In Proceedings of the 7th Python in Science Conference, 11-15.

Hale, T., Angrist, N., Goldszmidt, R., Kira, B., Petherick, A., Phillips, T., Webster, S., Cameron-Blake, E., Hallas, L., Majumdar, S., and Tatlow, H. (2021). A global panel database of pandemic policies (Oxford COVID-19 Government Response Tracker). Nature Human Behaviour, 5(4), 529-538.

Higgins, J. P. T., and Thompson, S. G. (2002). Quantifying heterogeneity in a meta-analysis. Statistics in Medicine, 21(11), 1539-1558.

Higgins, J. P. T., Thompson, S. G., Deeks, J. J., and Altman, D. G. (2003). Measuring inconsistency in meta-analyses. BMJ, 327(7414), 557-560.

IntHout, J., Ioannidis, J. P. A., Rovers, M. M., and Goeman, J. J. (2016). Plea for routinely presenting prediction intervals in meta-analysis. BMJ Open, 6(7), e010247.

Kissler, S. M., Tedijanto, C., Goldstein, E., Grad, Y. H., and Lipsitch, M. (2020). Projecting the transmission dynamics of SARS-CoV-2 through the postpandemic period. Science, 368(6493), 860-868.

Knapp, G., and Hartung, J. (2003). Improved tests for a random effects meta-regression with a single covariate. Statistics in Medicine, 22(17), 2693-2710.

Kraemer, M. U. G., Yang, C.-H., Gutierrez, B., Wu, C.-H., Klein, B., Pigott, D. M., et al. (2020). The effect of human mobility and control measures on the COVID-19 epidemic in China. Science, 368(6490), 493-497.

Kuramoto, Y. (1984). Chemical oscillations, waves, and turbulence. Springer.

Lachaux, J.-P., Rodriguez, E., Martinerie, J., and Varela, F. J. (1999). Measuring phase synchrony in brain signals. Human Brain Mapping, 8(4), 194-208.

Mantel, N. (1967). The detection of disease clustering and a generalized regression approach. Cancer Research, 27(2), 209-220.

Mathieu, E., Ritchie, H., Ortiz-Ospina, E., Roser, M., Hasell, J., Appel, C., Giattino, C., and Rodés-Guirao, L. (2021). A global database of COVID-19 vaccinations. Nature Human Behaviour, 5(7), 947-953.

Mathieu, E., Ritchie, H., Rodés-Guirao, L., Appel, C., Giattino, C., Hasell, J., Macdonald, B., Dattani, S., Beltekian, D., Ortiz-Ospina, E., and Roser, M. (2020). Coronavirus pandemic (COVID-19). Our World in Data.

Neher, R. A., Dyrdak, R., Druelle, V., Hodcroft, E. B., and Albert, J. (2020). Potential impact of seasonal forcing on a SARS-CoV-2 pandemic. Swiss Medical Weekly, 150, w20224.

Newman, M. E. J. (2006). Modularity and community structure in networks. Proceedings of the National Academy of Sciences, 103(23), 8577-8582.

Nyberg, T., Ferguson, N. M., Nash, S. G., Webster, H. H., Flaxman, S., Andrews, N., et al. (2022). Comparative analysis of the risks of hospitalisation and death associated with SARS-CoV-2 omicron (B.1.1.529) and delta (B.1.617.2) variants in England. The Lancet, 399(10332), 1303-1312.

Page, M. J., McKenzie, J. E., Bossuyt, P. M., Boutron, I., Hoffmann, T. C., Mulrow, C. D., et al. (2021). The PRISMA

2020 statement: An updated guideline for reporting systematic reviews. BMJ, 372, n71.

Pastor-Satorras, R., Castellano, C., Van Mieghem, P., and Vespignani, A. (2015). Epidemic processes in complex networks. Reviews of Modern Physics, 87(3), 925-979.

Pikovsky, A., Rosenblum, M., and Kurths, J. (2001). Synchronization: A universal concept in nonlinear sciences. Cambridge University Press.

Rohani, P., Earn, D. J. D., and Grenfell, B. T. (1999). Opposite patterns of synchrony in sustained oscillations of measles and whooping cough. Science, 286(5441), 968–971.

Rosenblum, M. G., Pikovsky, A. S., and Kurths, J. (1996). Phase synchronization of chaotic oscillators. Physical Review Letters, 76(11), 1804-1807.

Sakoe, H., and Chiba, S. (1978). Dynamic programming algorithm optimization for spoken word recognition. IEEE Transactions on Acoustics, Speech, and Signal Processing, 26(1), 43-49.

Schreiber, T., and Schmitz, A. (2000). Surrogate time series. Physica D, 142(3-4), 346-382.

Tegally, H., Wilkinson, E., Giovanetti, M., Iranzadeh, A., Fonseca, V., Giandhari, J., et al. (2021). Detection of a SARS-CoV-2 variant of concern in South Africa. Nature, 592(7854), 438-443.

Theiler, J., Eubank, S., Longtin, A., Galdrikian, B., and Farmer, J. D. (1992). Testing for nonlinearity in time series: The method of surrogate data. Physica D, 58(1-4), 77-94.

Torrence, C., and Compo, G. P. (1998). A practical guide to wavelet analysis. Bulletin of the American Meteorological Society, 79(1), 61-78.

Torrence, C., and Webster, P. J. (1999). Interdecadal changes in the ENSO–monsoon system. Journal of Climate, 12(8), 2679-2690.

Viana, R., Moyo, S., Amoako, D. G., Tegally, H., Scheepers, C., Althaus, C. L., et al. (2022). Rapid epidemic expansion of the SARS-CoV-2 Omicron variant in southern Africa. Nature, 603(7902), 679-686.

Viboud, C., Bjørnstad, O. N., Smith, D. L., Simonsen, L., Miller, M. A., and Grenfell, B. T. (2006). Synchrony, waves, and spatial hierarchies in the spread of influenza. Science, 312(5772), 447-451.

Viechtbauer, W. (2005). Bias and efficiency of meta-analytic variance estimators in the random-effects model. Journal of Educational and Behavioral Statistics, 30(3), 261-293.

Virtanen, P., Gommers, R., Oliphant, T. E., Haberland, M., Reddy, T., Cournapeau, D., et al. (2020). SciPy 1.0: Fundamental algorithms for scientific computing in Python. Nature Methods, 17(3), 261-272.

Volz, E., Mishra, S., Chand, M., Barrett, J. C., Johnson, R., Geidelberg, L., et al. (2021). Assessing transmissibility of SARS-CoV-2 lineage B.1.1.7 in England. Nature, 593(7858), 266-269.

Yule, G. U. (1926). Why do we sometimes get nonsense-correlations between time-series? A study in sampling and the nature of time-series. Journal of the Royal Statistical Society, 89(1), 1-63.